

# UNCLASSIFIED

AD NUMBER
AD482099
NEW LIMITATION CHANGE
TO Approved for public release, distribution unlimited
FROM Distribution authorized to U.S. Gov't. agencies and their contractors; Critical Technology; JAN 1966. Other requests shall be referred to Air Force Systems Command, Space Systems Div., Los Angeles, CA.
AUTHORITY
SAMSO ltr, 24 Jan 1972

THIS PAGE IS UNCLASSIFIED

AD 482099

## Static and Dynamic Oxidation of ZrC

JANUARY 1966

*Prepared by K.R. JANOWSKI, R.D. CARNAHAN and R.C. ROSSI  
Materials Sciences Laboratory*

*Prepared for BALLISTIC SYSTEMS AND SPACE SYSTEMS DIVISIONS*

**AIR FORCE SYSTEMS COMMAND  
LOS ANGELES AIR FORCE STATION  
Los Angeles, California**



LABORATORY OPERATIONS • AEROSPACE CORPORATION  
CONTRACT NO. AF 04(695)-669

**Best Available Copy**

## NOTICE

This document is subject to special export controls and each transmittal to foreign governments or foreign nationals may be made only with prior approval of SSD (SSTR T).

SSD-TR-66-33

Report No.  
TDR-669(6250-10)-3

STATIC AND DYNAMIC OXIDATION OF ZrC

Prepared by

K. R. Janowski  
R. D. Carnahan  
R. C. Rossi  
Materials Sciences Laboratory

Laboratory Operations  
AEROSPACE CORPORATION  
El Segundo, California

Contract No. AF 04(695)-669


January 1966

Prepared for

BALLISTIC SYSTEMS AND SPACE SYSTEMS DIVISIONS  
AIR FORCE SYSTEMS COMMAND  
LOS ANGELES AIR FORCE STATION  
Los Angeles, California

STATIC AND DYNAMIC OXIDATION OF ZrC


Prepared


  
R. R. Janowski

  
R. C. Rossi

R. D. Carnahan

Approved

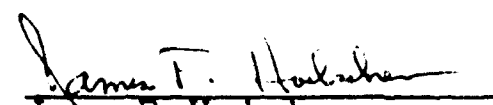
  
E. G. Kendall, Head  
Metallurgy and Ceramics  
Department

  
W. C. Riley, Associate Director  
Materials Sciences Laboratory

  
J. E. Hove, Director  
Materials Sciences Laboratory

This technical documentary report has been reviewed and is approved for publication and dissemination. The conclusions and findings contained herein do not necessarily represent an official Air Force position.

For Space Systems Division  
Air Force Systems Command

  
James F. Hoelscher  
Captain, USAF

## ABSTRACT

The purpose of this laboratory experiment was to determine the oxidation characteristics of ZrC, both as a monocarbide and in combination with free carbon. The oxidation tests conducted were twofold: a static test run in still air and a dynamic test using a high-velocity air blast.

It was found that the oxidation behavior of single-phased ZrC and ZrC + C is a function of the C concentration. At lower temperatures, increasing the C content decreases the resistance to oxidation. It was also discovered that adding alloying elements had little effect on either the static or the dynamic oxidation behaviors.

## CONTENTS

I.	INTRODUCTION . . . . .	1
II.	EXPERIMENTAL PROCEDURE . . . . .	3
III.	RESULTS . . . . .	11
	A. Static Oxidation . . . . .	11
	B. Dynamic Oxidation . . . . .	13
IV.	DISCUSSION . . . . .	21
	A. Effect of Carbon . . . . .	21
	B. Effect of Alloying Additions . . . . .	26
	C. Effect of Iron . . . . .	26
	D. Comparison of ZrC and W . . . . .	28
V.	CONCLUSIONS . . . . .	31
	REFERENCES . . . . .	33

## FIGURES

1.	Zirconium-Carbon Phase Diagram . . . . .	4
2.	Arc-Casting Furnace Schematic Diagrams . . . . .	5
3.	Oxidation Test Equipment . . . . .	8
4.	Recession Rate vs Temperature for ZrC and ZrC + C Under Static Test Conditions . . . . .	12
5.	Recession Rate of ZrC and ZrC + C at Different Temperatures Under Static Test Conditions. . . . .	14
6.	Recession Rate vs Temperature for Alloyed ZrC + C Under Static Test Conditions. . . . .	15
7.	Recession Rate vs Temperature for ZrC and ZrC + C Under Dynamic Test Conditions. . . . .	16
8.	Recession Rate vs Temperature for Alloyed ZrC + C Under Dynamic Test Conditions. . . . .	18
9.	ZrC + 5 a/o B Dynamic Oxidation Specimens. . . . .	20
10.	Oxidation of Hypoeutectic ZrC . . . . .	22
11.	Oxidation of Hypereutectic ZrC . . . . .	23
12.	Recession Rate vs $1/T$ for ZrC and ZrC + C . . . . .	25
13.	Oxidation of Intergranular $Fe_3C$ in ZrC Matrix . . . . .	27
14.	Comparison of Recession Rates of 19 w/o C ZrC with Pure W and W + 10 v/o $Al_2O_3$ . . . . .	29



## TABLES

1.	Recession Rates of Hot-Pressed ZrC . . . . .	11
2.	Static Tests of ZrC Specimens . . . . .	13
3.	Recession Rates of Unalloyed ZrC . . . . .	17
4.	Dynamic Oxidation Results of Alloyed ZrC . . . . .	17

## I. INTRODUCTION<sup>\*</sup>

The carbides of the metals in Groups 4 and 5 are among the materials having the highest melting point. The application of these materials has been limited primarily because of a lack of information concerning the properties of the base carbide, as well as of an understanding of the effects of other chemical species on the properties.

The purpose of this study was to determine the oxidation characteristics of  $\text{ZrC}$ , both as the monocarbide and in combination with free carbon. An additional purpose was to attempt to alter the oxidation behavior by the addition of alloying elements.

Oxidation specimens were prepared both by melting techniques and by hot pressing. The oxidation tests were of two types: (1) a static test run in still air, and (2) a dynamic test using a high-velocity air blast. The oxidation resistance was determined on the carbide with different carbon compositions and  $\text{ZrC}+\text{C}$ , to which has been added Ta, B, Cr, and  $\text{ThO}_2$ .

---

<sup>\*</sup> R. D. Carnahan is presently with Handy & Harman, Fairfield, Conn.

## II. EXPERIMENTAL PROCEDURE

The ZrC specimens used in these tests were prepared by two different techniques: vacuum arc melting and hot pressing. The initial step in the processing was the fusion of reactor grade Zr sponge from Wah Chang with National Carbon Company AGOT grade graphite. Chemical analyses of the Zr sponge indicate that the only impurity elements found in concentrations greater than 100 ppm are Fe, Cl, Mg, and O. Grade AGOT graphite is a high purity nuclear graphite.

The Zr-C binary equilibrium diagram is shown in Fig. 1. In the initial melting and homogenizing process, the C content was adjusted to approximately 22 w/o C, slightly hypereutectic in carbon composition. After homogenization, the carbide was crushed to -8 mesh and was stored to be used as melting stock. Alloying was done in an arc-melting furnace using a graphite mold and electrode, as shown in Fig. 2. Carbon content was controlled by the addition of Zr sponge or graphite. The carbon contents of the unalloyed arc-melted ZrC investigated ranged from 19 w/o C (hypoeutectic) to 23 w/o C. Alloying elements added to the arc-melted carbide included Cr and Ta, both added in the elemental state. In the alloying studies, the C content was held constant at 22 w/o while Cr or Ta was added.

The ZrC used in the hot-pressing studies was prepared by ball milling the -8 mesh ZrC (22 w/o C) in a stainless steel ball mill using kerosene as the liquid vehicle. Ball-milling reduced the carbide to -250 mesh. It was found that the overall C content was reduced during the ball milling operation since the carbide fractured along the weakest planes, i.e., the graphite flakes in the structure. The free graphite was then picked up in the kerosene and floated off during the alcohol rinse. The C content after ball milling was about 20 w/o. It was also found that the ball milling operation resulted in the pickup of impurities

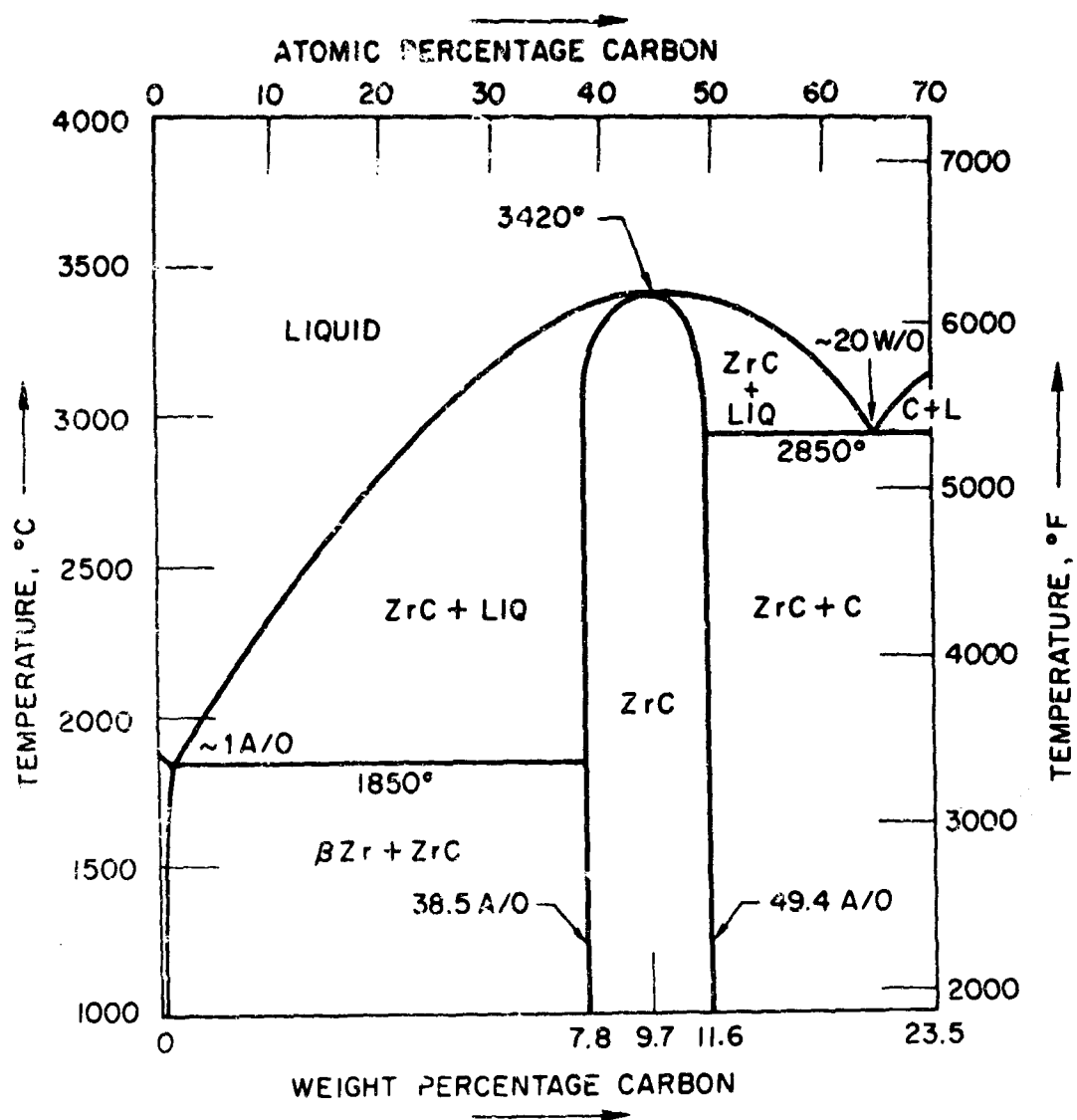


Fig. 1. Zirconium-Carbon Phase Diagram

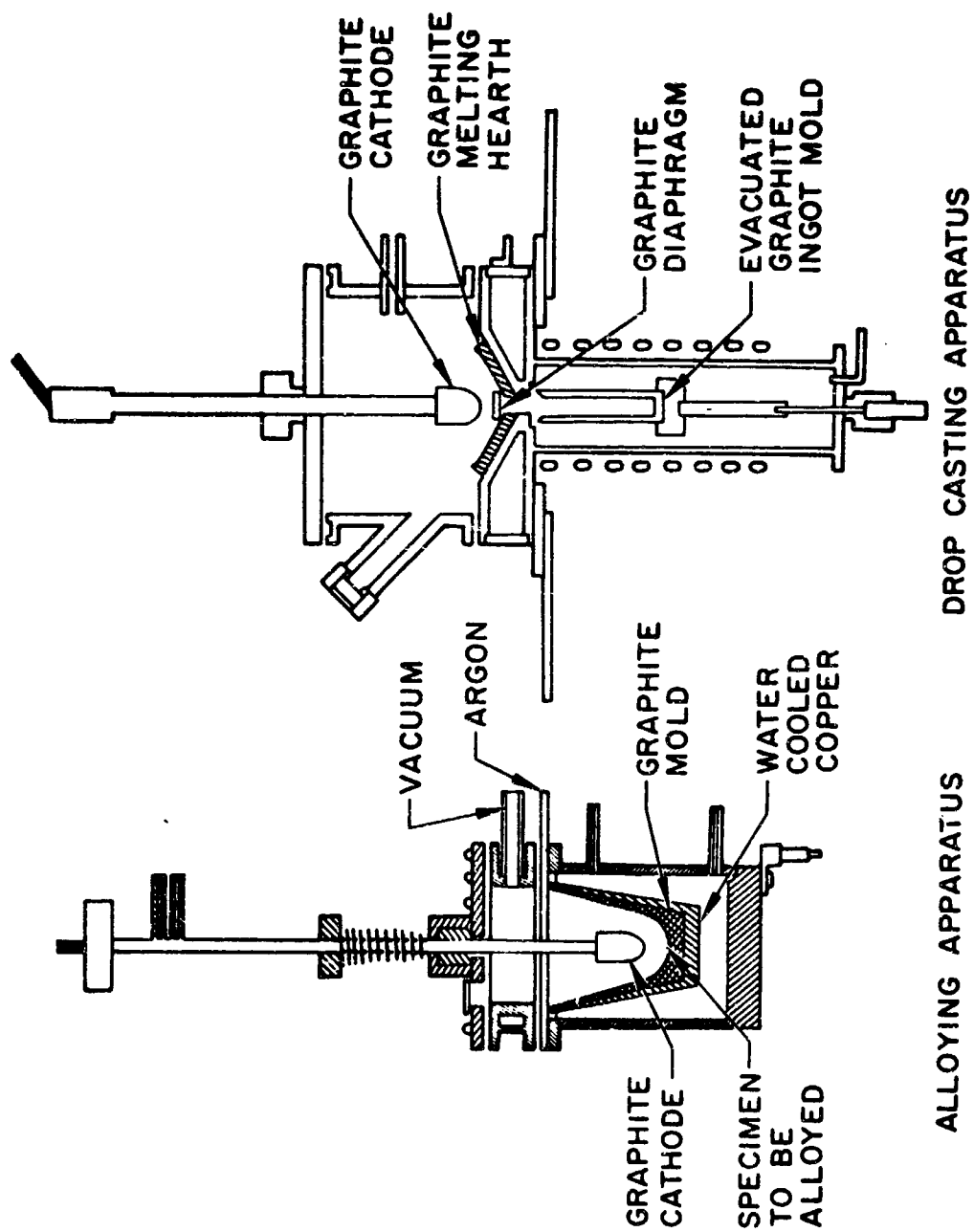


Fig. 2. Arc-Casting Furnace Schematic Diagrams

due to the abrasive action of the carbide on the stainless steel mill and balls. The principal impurity was Fe (about 1 v/o), which was found in the microstructure as  $\text{Fe}_3\text{C}$ . To determine the effect of Fe on the oxidation behavior, ZrC, which had been leached in HCl to remove the Fe, was also tested and compared with Fe-contaminated ZrC.

Carbon content in the hot-pressed ZrC was varied by adding either AGOT graphite (-250 mesh) or Zr powder ( $3\ \mu$ ). The Zr was added in an argon atmosphere to reduce oxygen pickup. The powders were mixed by dry-blending. The alloying additions to the hot-pressed ZrC included Cr, Ta, B, and  $\text{ThO}_2$ . The Cr was added as  $\text{Cr}_3\text{C}_2$ , Ta as TaC, and B as  $\text{ZrB}_2$  and  $\text{B}_4\text{C}$ . All these powders were -150 mesh. The  $\text{ThO}_2$  was added as  $3\ \mu$  powder.

Hot-pressing was performed in an induction-heated graphite die. A total of 6000 psi pressure was applied through two hydraulic rams above  $1000^\circ\text{C}$ . Heating continued to the final pressing temperature  $2200^\circ\text{C}$ , where the sample was held for 30 min; the pressure was then released and the induction unit was turned off.

Static oxidation specimens were cut from the carbide billets using a diamond saw. The specimens were in the form of right parallel-piped, approximately  $1/8$  by  $1/8$  by  $3/8$  in. Both static and dynamic specimens were degreased after machining, but prior to testing.

The length, width, and height of the specimens were measured to four significant figures before testing; the specimens were weighed to five significant figures. Oxidation was carried out in a platinum-wound alumina tube furnace, both ends of the tube being open. The specimens were placed in a platinum boat, were allowed to reach the test temperature as determined by a micro-optical pyrometer, and were held at that temperature for 15 min. Test temperatures ranged from 600 to  $1200^\circ\text{C}$ . The specimens were removed from the furnace, were allowed to cool, and were weighed. The oxide was carefully removed,

and the specimens were remeasured. Recession rates were determined from the change in dimensions. These are recorded in the dimensions of mils/second (thousandths of an inch recession/second).

The specimens for the dynamic tests were machined by coring 1/4 in. diam cylinders from the billets with a diamond core drill. The final lengths were approximately 1-1/4 in. The same dimensions of recession rate were used for the dynamic tests. In these tests, however, the specimens were heated by self-resistance and were oxidized by an air blast. The oxidation test fixture is shown in Fig. 3. The sample was gripped by two water-cooled Cu grips (as shown in the lower right part of the figure), thus completing the dc circuit. After the test temperature was attained, the protective flow of argon was stopped and the 136 ft/sec ( $44 \text{ in}^3/\text{sec}$ ) air blast was started. Specimens were run for 5 min, after which the air blast was shut off and the argon flow resumed as the specimen was cooled. One modification to Fig. 3 was employed for use with carbides.

Due to the buildup of oxide layers and due to uncertainties in emissivities, it was decided to use a system of temperature measurement utilizing nearly black body conditions, rather than to read the temperature from the side of the specimen with the micro-optical pyrometer, as shown in Fig. 3. To do this, a hole was drilled in the end plate of the test fixture, and sight holes were machined in the carbide specimens by means of spark-discharge machining. Blind holes were machined in both ends of the cylinders, leaving approximately a 1/16-in. web of carbide. Micro-optical pyrometer readings were taken from this web during the tests. The depth-to-diameter ratios of the holes approximated black body conditions, and accurate temperature readings were obtained.

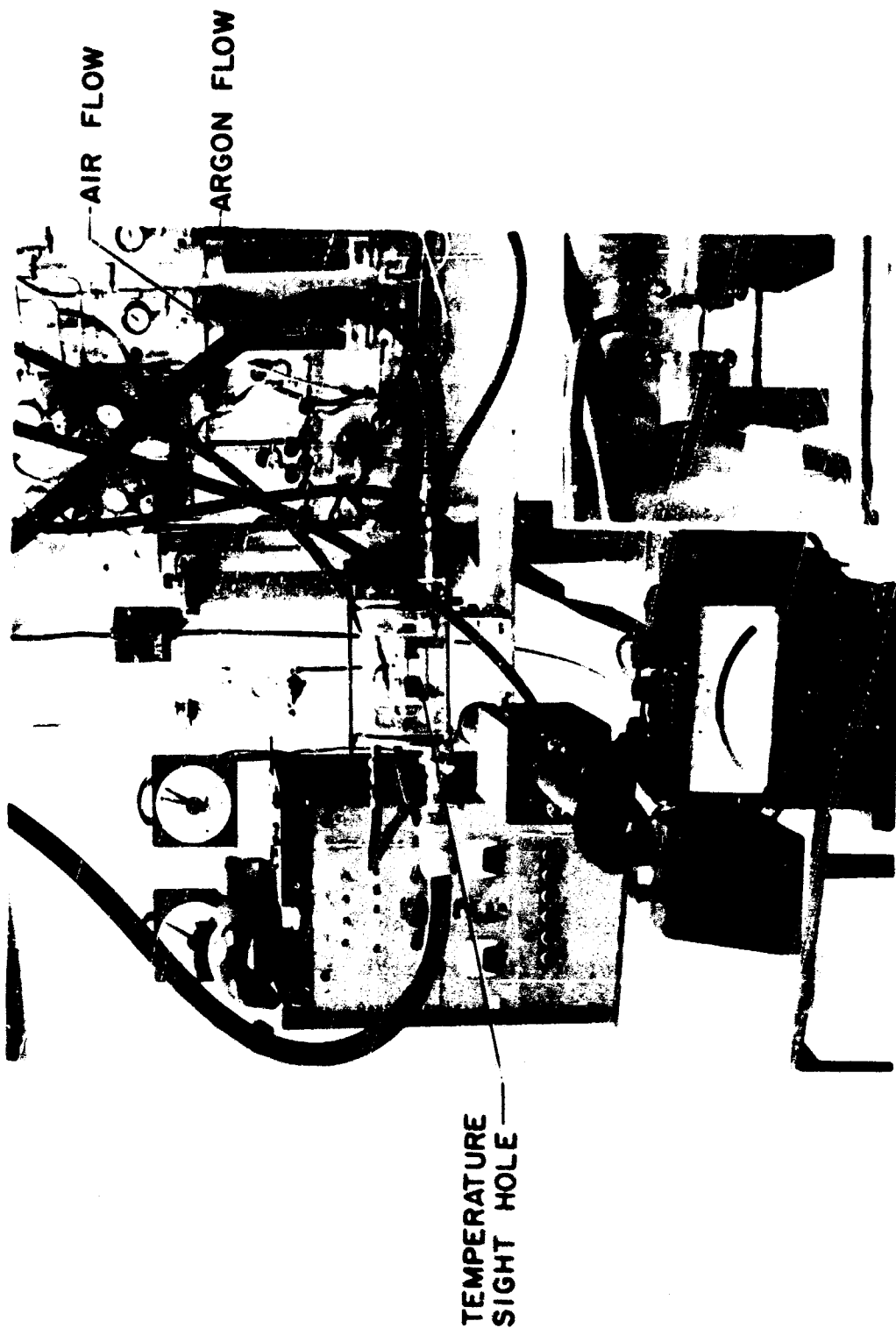


Fig. 3. Oxidation Test Equipment



Dynamic test temperatures utilized were from 1600 to 2800°C. After testing, the cylinders were mounted in acrylic plastic plugs, were sectioned with a jeweler's diamond saw, and were polished metallographically. The diameters of the cylinders, which had been measured to four significant figures prior to testing, were measured again microscopically, both parallel and normal to the air flow direction, and recession rates were again determined. The recession rates did not vary significantly parallel and normal to the air flow; hence, the rates given are averages of the two directions.

### III. RESULTS

#### A. STATIC OXIDATION

The recession rates of the hot-pressed ZrC with no alloying additions are listed in Table 1:

Table 1. Recession Rates of Hot-Pressed ZrC

w/o carbon	Recession Rate, mils/sec		
	800°C	1000°C	1200°C
8.8	-	$1.5 \times 10^{-3}$	$1.8 \times 10^{-3}$
11.7	$1.1 \times 10^{-3}$	$3.8 \times 10^{-3}$	$4.5 \times 10^{-3}$
15.5	-	$4.4 \times 10^{-3}$	$4.8 \times 10^{-3}$
20.0	$4.7 \times 10^{-3}$	$8.4 \times 10^{-3}$	$8.0 \times 10^{-3}$
22.0	$7.9 \times 10^{-3}$	$1.0 \times 10^{-2}$	$1.1 \times 10^{-2}$
25.0	-	-	$1.4 \times 10^{-2}$

The data are plotted in Figs. 4 and 5. From Fig. 1 it can be seen that the 8.8 w/o C and 11.7 w/o C are near the extreme composition limits of the single-phased ZrC field. The results of the static tests indicate that the resistance to oxidation is a function of the composition in this range, i. e., the lower the C content, the better the oxidation resistance. This same behavior is noted in the two-phased ZrC + C region, where the recession rate increases with increasing C content. The difference between the two C extremes in the monocarbide is more marked, however, than the difference between single- and two-phased structures, as can be seen in Fig. 4. In the higher C content structures no significant difference was observed in recession rates between 1000 and 1200°C.

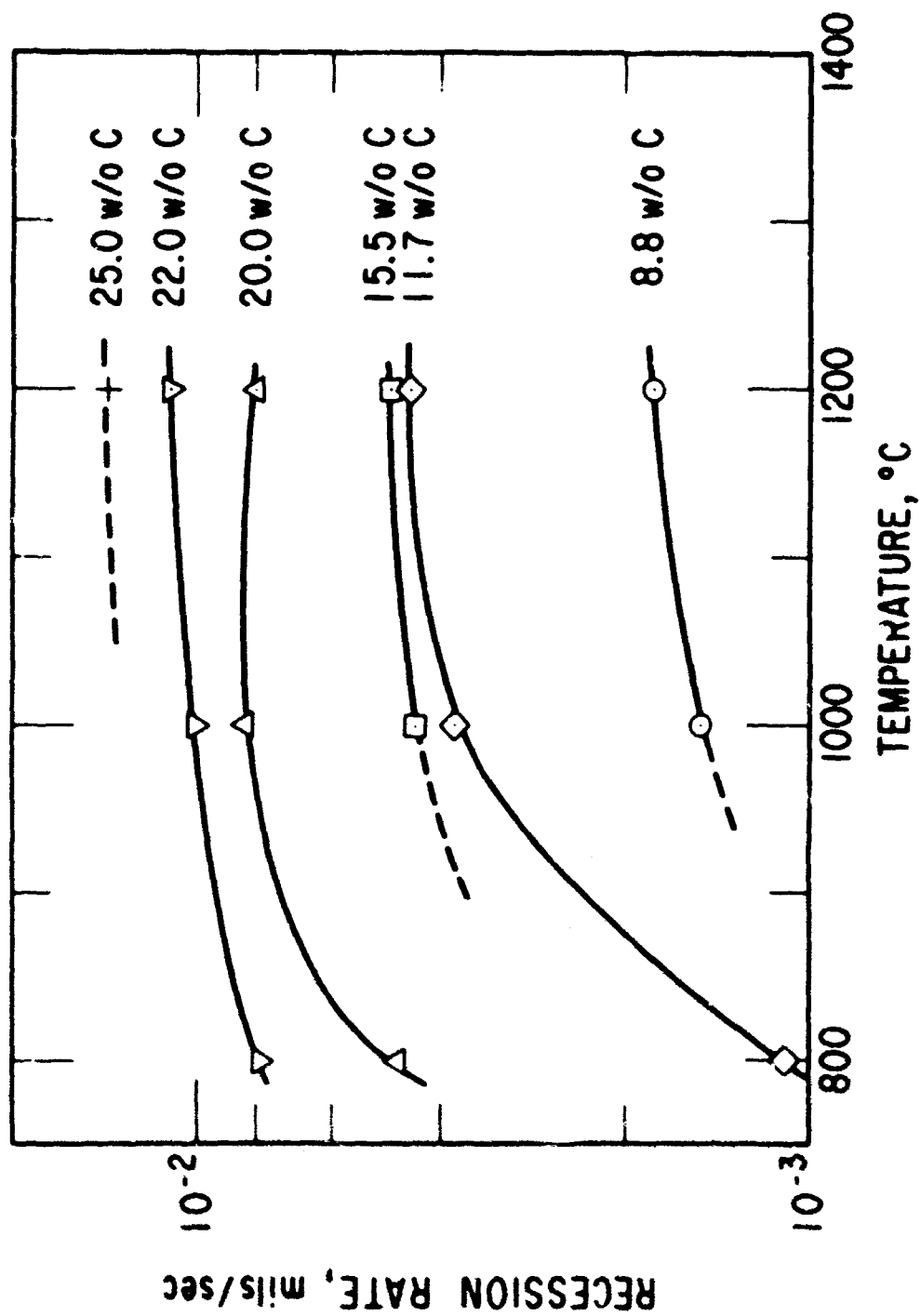


Fig. 4. Recession Rate vs Temperature for ZrC and ZrC + C Under Static Test Conditions

In Fig. 5 the data are plotted as a function of carbon content for the test temperatures investigated. There appears to be only a small difference between the recession rates at 1000 and 1200°C as compared with the 800°C tests.

The static tests of the alloyed hot-pressed ZrC specimens are listed in Table 2 and are shown in Fig. 6:

Table 2. Static Tests of ZrC Specimens

Alloy Percentage (ZrC=20 w/o C)	Recession Rate, mils/sec		
	800°C	1000°C	1200°C
1 a/o B (ZrB <sub>2</sub> )	$5.1 \times 10^{-3}$	$5.9 \times 10^{-3}$	$8.3 \times 10^{-3}$
10 a/o B (ZrB <sub>2</sub> )	$2.3 \times 10^{-3}$	$5.0 \times 10^{-3}$	$9.7 \times 10^{-3}$
1 a/o B (B <sub>4</sub> C)	$5.6 \times 10^{-3}$	$7.3 \times 10^{-3}$	$8.9 \times 10^{-3}$
5 a/o B (B <sub>4</sub> C)	$6.2 \times 10^{-3}$	$6.5 \times 10^{-3}$	$8.6 \times 10^{-3}$
1 a/o Ta	$3.6 \times 10^{-3}$	$5.6 \times 10^{-3}$	$8.6 \times 10^{-3}$
5 a/o Ta	$2.9 \times 10^{-3}$	$3.4 \times 10^{-3}$	$1.0 \times 10^{-2}$
1 a/o Cr	$4.9 \times 10^{-3}$	$7.1 \times 10^{-3}$	$9.1 \times 10^{-3}$
5 a/o Cr	$7.3 \times 10^{-3}$	$8.8 \times 10^{-3}$	$1.0 \times 10^{-2}$

The recession rate of the base 20 w/o C ZrC is shown in Fig. 6, along with the effects of the alloying additions. The alloyed carbides show no consistent behavior with alloying constituent. The spread in recession rate is much greater at 600 and 800°C than at 1200°C, where all the alloyed carbides have a greater recession rate than the base carbide.

#### B. DYNAMIC OXIDATION

The recession rates of the unalloyed ZrC run under dynamic oxidation conditions are listed in Table 3 and are shown in Fig. 7.

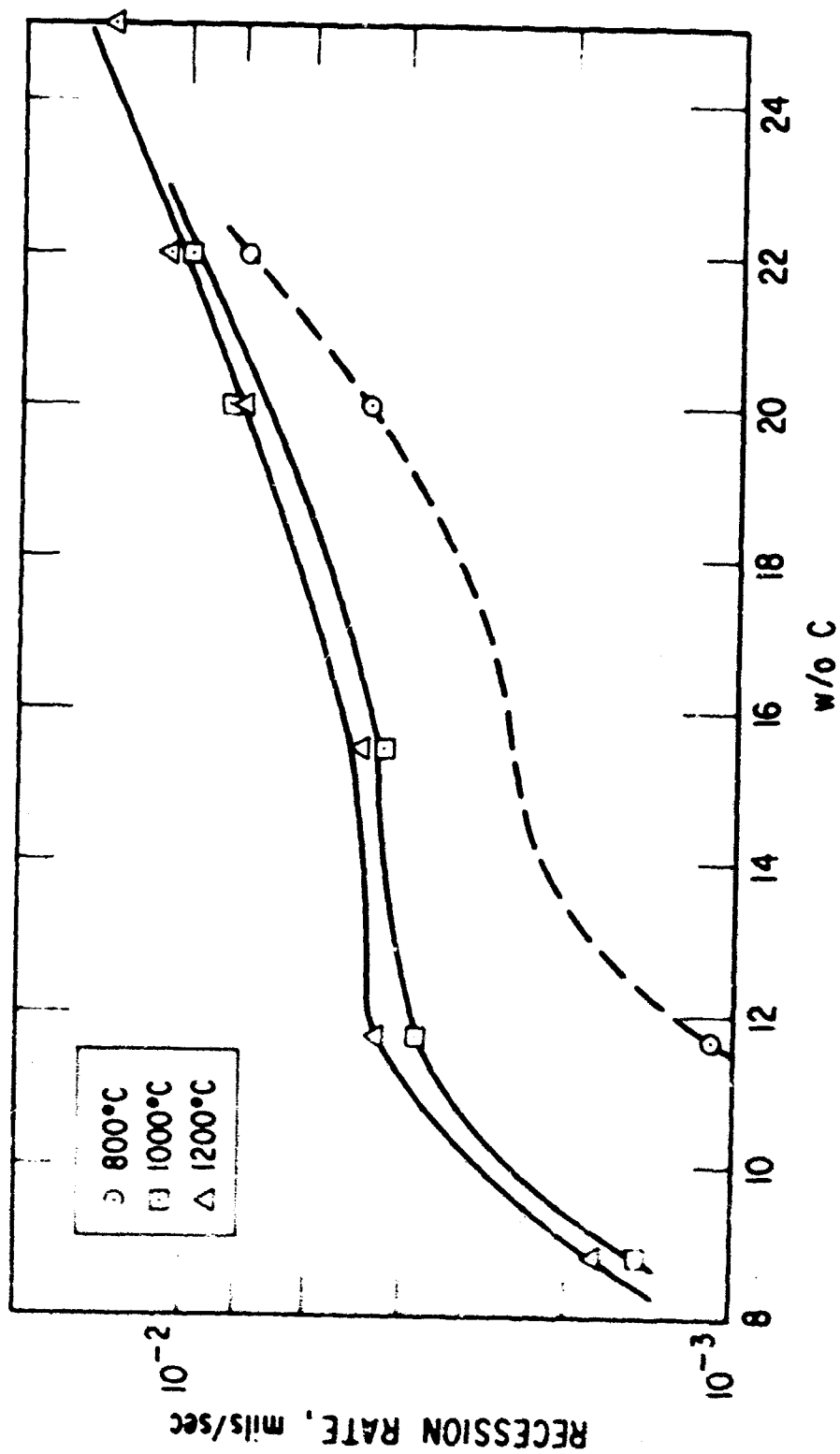


Fig. 5. Recession Rate of ZrC and ZrC + C at Different Temperatures Under Static Test Conditions

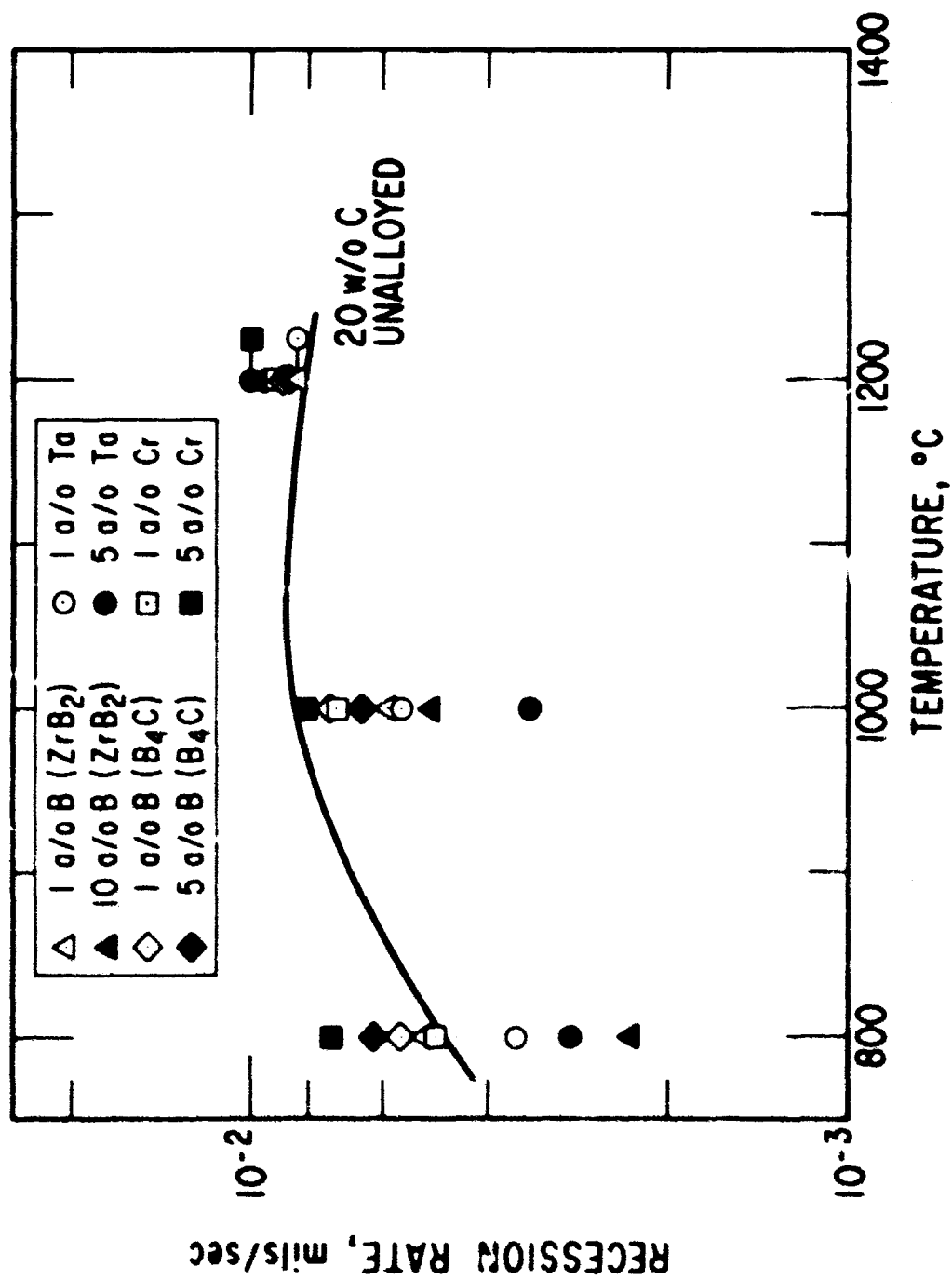


Fig. 6. Recession Rate vs Temperature for Alloyed ZrC + C Under Static Test Conditions

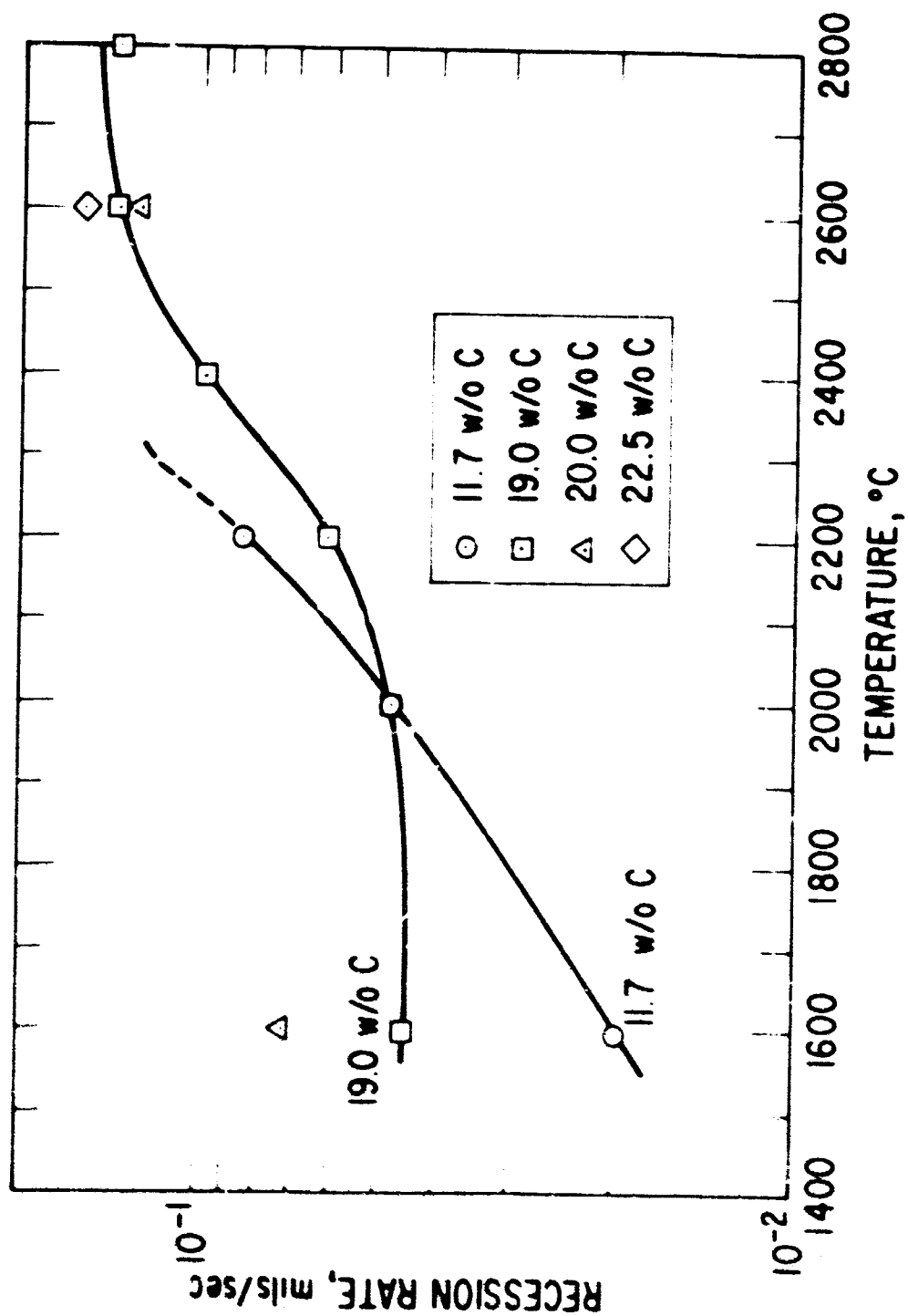


Fig. 7. Recession Rate vs Temperature for ZrC and ZrC + C Under Dynamic Test Conditions

Table 3. Recession Rates of Unalloyed ZrC

w/o C	Recession Rate, mils/sec					
	1600°C	2000°C	2200°C	2400°C	2600°C	2800°C
11.7 (hot pressed)	$2.0 \times 10^{-2}$	$4.7 \times 10^{-2}$	$8.5 \times 10^{-2}$	-	-	-
19.0 (arc melted)	$4.5 \times 10^{-2}$	$4.7 \times 10^{-2}$	$6.0 \times 10^{-2}$	$1.0 \times 10^{-1}$	$1.4 \times 10^{-1}$	$1.4 \times 10^{-1}$
20.0 (arc melted)	$7.3 \times 10^{-2}$	-	-	-	$1.3 \times 10^{-1}$	-
22.5 (arc melted)	-	-	-	-	$1.6 \times 10^{-1}$	-

At 1600°C there appears to be the same relationship between carbon content and recession rate as was observed in the static tests, i.e., an increase in recession rate with increasing carbon content. However, this behavior is reversed at higher temperatures where the carbide containing the higher carbon content shows lower recession rates.

The dynamic oxidation results of the alloyed ZrC are listed in Table 4 and are shown in Fig. 8:

Table 4. Dynamic Oxidation Results of Alloyed ZrC

Alloy % (ZrC=19.7 w/o C)	Oxidation Test Temperatures					
	1600°C	1800°C	2000°	2200°C	2400°C	2600°C
1 a/o Cr <sup>a</sup>	-	$6.0 \times 10^{-2}$	-	$7.0 \times 10^{-2}$	-	$1.5 \times 10^{-1}$
2.2 a/o Ta	$5.2 \times 10^{-2}$	$4.9 \times 10^{-2}$	$5.3 \times 10^{-2}$	$9.4 \times 10^{-2}$	$1.6 \times 10^{-1}$	-
5 a/o B(B <sub>4</sub> C)	$6.6 \times 10^{-2}$	$7.6 \times 10^{-2}$	$7.4 \times 10^{-2}$	$1.0 \times 10^{-1}$	$1.5 \times 10^{-1}$	-
5 v/o ThO <sub>2</sub>	$6.7 \times 10^{-2}$	$6.5 \times 10^{-2}$	$7.0 \times 10^{-2}$	$1.1 \times 10^{-1}$		

<sup>a</sup>Arc melted; remainder, hot pressed



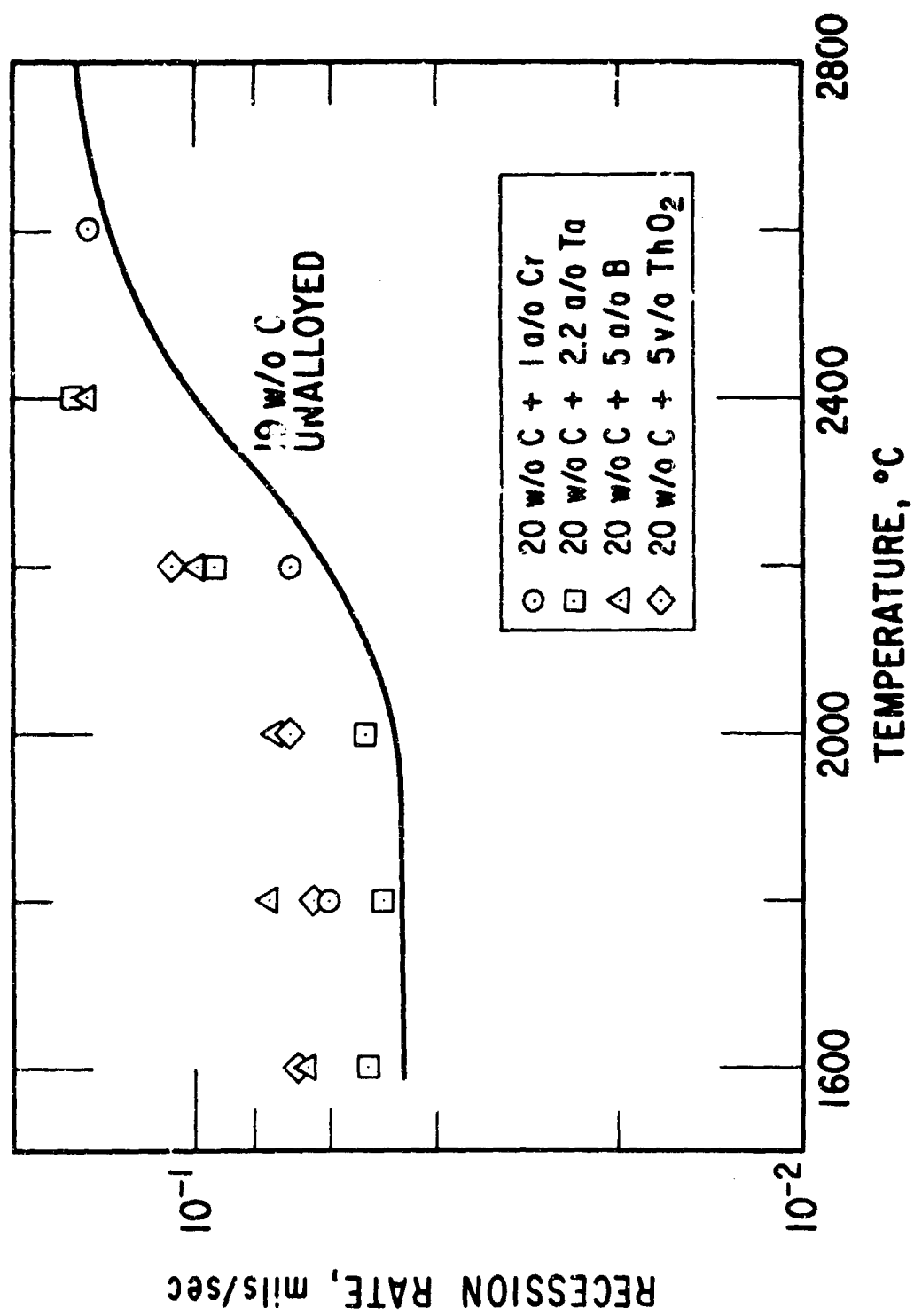


Fig. 8. Recession Rate vs Temperature for Aligned ZrC + C Under Dynamic Test Conditions

The alloyed data in Fig. 8 are shown with the recession rate curve from Fig. 7 for the 19.0 w/o C ZrC. In all cases, the recession rates for the alloyed carbides are greater than for the 19.0 w/o C ZrC but lower than the 20 w/o C value shown in Fig. 7. At lower temperatures, the ZrC containing Ta closely approaches the oxidation rate of the 19.0 w/o C ZrC. At higher temperatures, the Cr-alloyed carbide comes nearest to the unalloyed carbide in oxidation behavior.

Figure 9 shows the series of hot-pressed specimens containing B, both before and after sectioning. The specimens retain approximately their original diameter. However, after sectioning, it can be seen that an oxide shell exists, the thickness of which increases at higher temperatures.

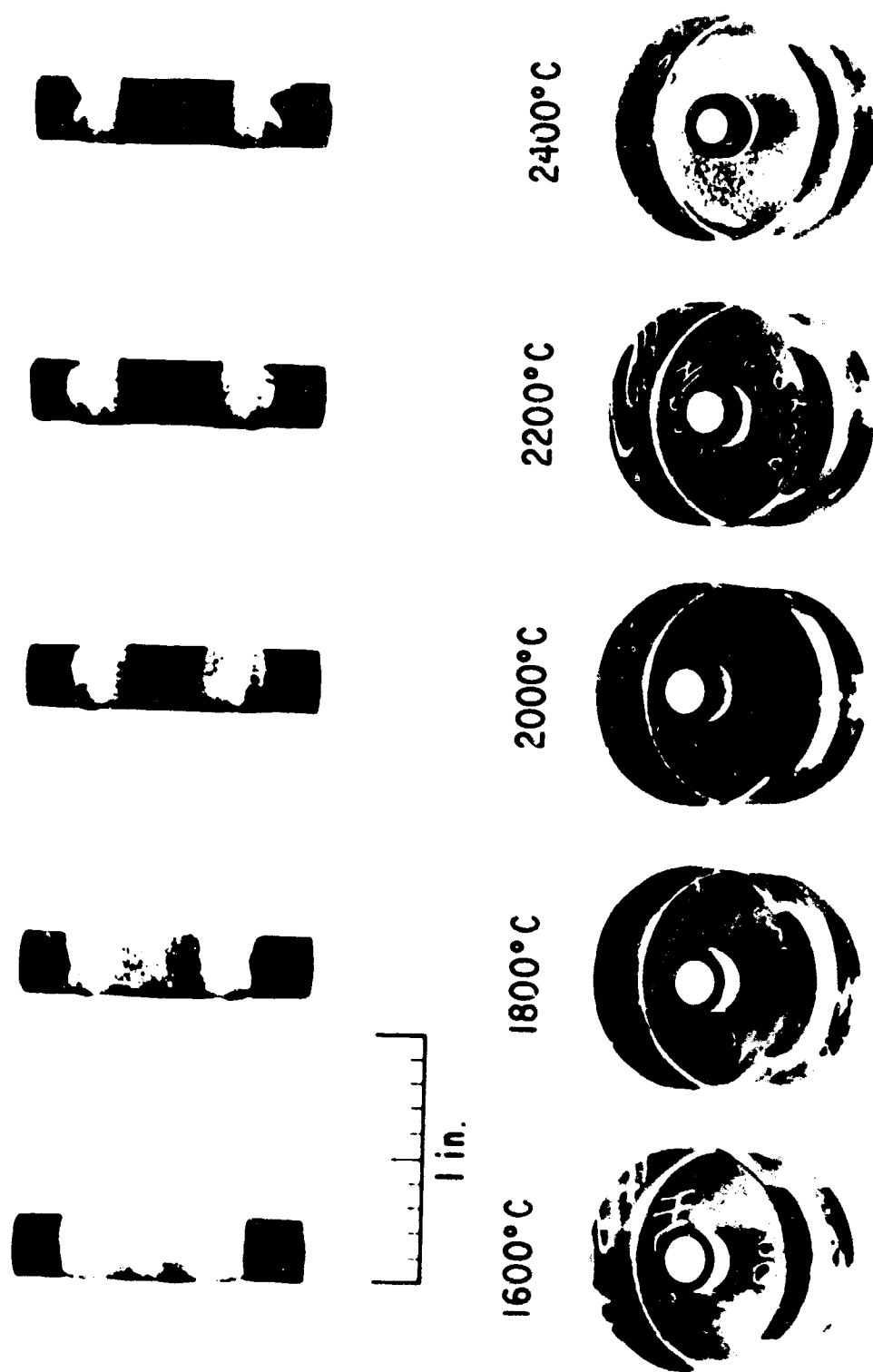


Fig. 9. ZrC + 5 a/o B Dynamic Oxidation Specimens

#### IV. DISCUSSION

##### A. EFFECT OF CARBON

Carbon appears in the microstructure of the carbides under consideration in three different ways, depending upon the overall carbon concentration. In the single-phase compound (7.8-11.6 w/o C), the carbon is chemically combined with the Zr in a monocarbide phase. In the hyperstoichiometric but hypoeutectic range (11.6-19.7 w/o C), the carbon appears as free graphite in the lamellar phase of the ZrC-C eutectic. Above 19.7 w/o C, the hypereutectic range, graphite is also present as free graphite flakes in addition to the lamellar constituent mentioned previously.

From a consideration of the static data it appears that the oxidation behavior of the single-phase ZrC is strongly dependent upon the percentage of C in the compound. As the structure becomes saturated in C, the resistance to oxidation decreases.

In the hypoeutectic region the microstructure consists of the ZrC phase saturated with C as well as with free lamellar graphite. As can be seen in Fig. 10, the graphite is attacked at a more rapid rate than the carbide, leaving isolated islands of ZrC in a matrix of oxide.

In the hypereutectic carbide the presence of graphite flakes promotes even more rapid oxidation of the microstructure. The graphite flakes in themselves have poor oxidation resistance, as is evident in Fig. 11. Moreover, as the flake is oxidized, a fresh carbide surface is exposed to the oxidizing environment, thereby enhancing the oxidation rate of the carbide-graphite eutectic matrix.

All these effects would increase the oxidation rates of ZrC as the carbon content is increased, as has been seen in both the static and dynamic oxidation behaviors.



100μ

Fig. 10. Oxidation of Hypoeutectic ZrC

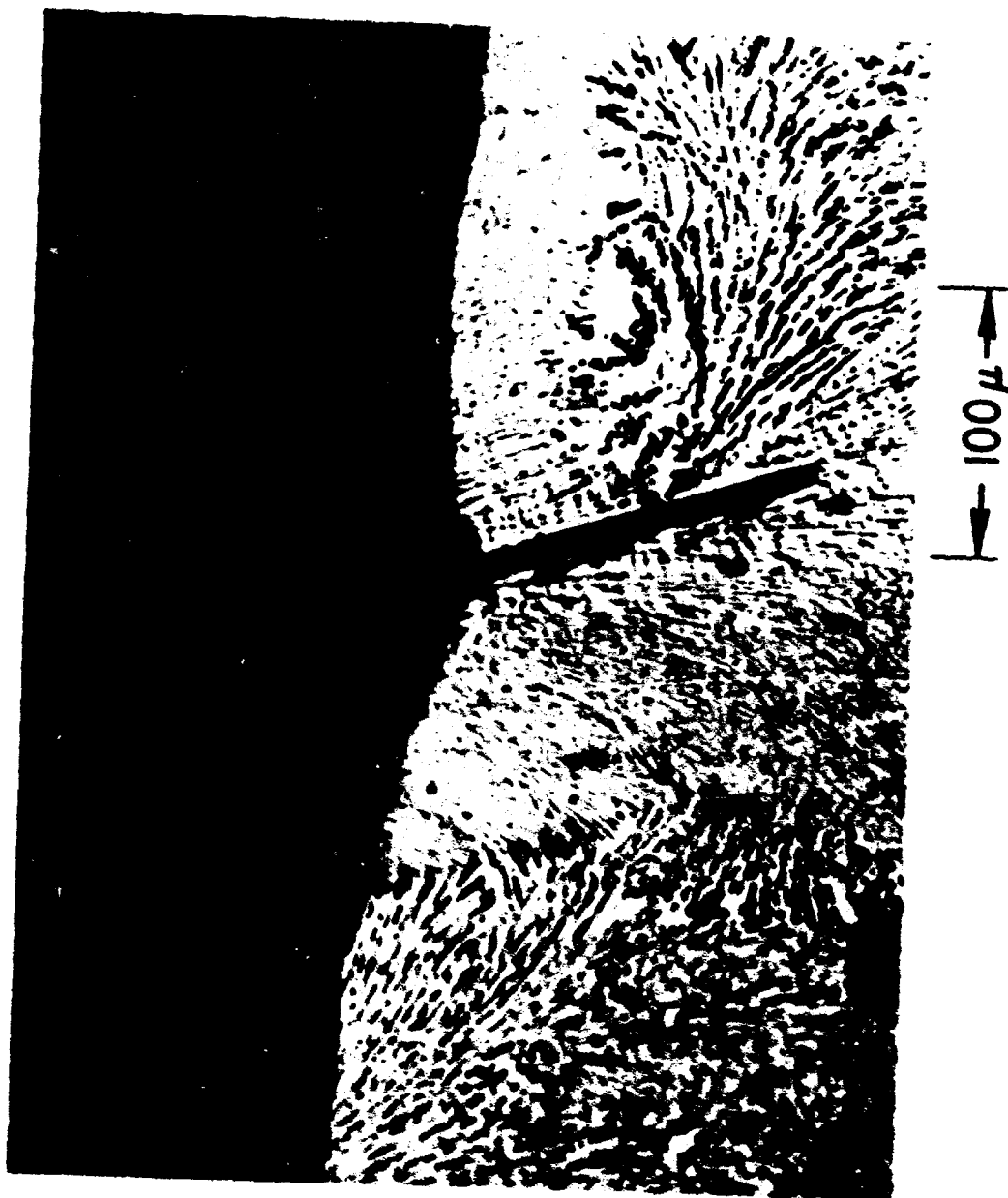


Fig. 11. Oxidation of Hypereutectic ZrC

At higher temperatures, the presence of C can actually improve the oxidation resistance, as can be seen by comparing the recession rates of the 11.7 w/o C and 19.0 w/o C under dynamic conditions (Fig. 7). At low temperatures, as stated previously, the presence of free C decreases the resistance to oxidation. As the temperature is increased, the rate of oxide buildup increases, resulting in quite heavy oxide layers (see Fig. 9). Thus, the effusion of oxygen through the oxide layer may be rate-controlling as the temperature increases. This explanation would account for the recession rate curves above about 2400°C. In addition, as the C content is increased, the reaction product gas CO must leave the surface of the carbide, resulting in a counter effusion.

At low temperatures, this is not a problem due to the relatively thin surface oxide layer. However, as the temperature is increased and the oxide thickness also increases, a barrier to the diffusion of CO is set up. Thus, an effective protective blanket of CO exists within the porous oxide phase and the amount of oxygen able to react with the carbide decreases. Thus, it is seen in Fig. 7 that the recession rate for 11.7 w/o C ZrC is greater at 2200°C than for 19.0 w/o C ZrC, where this protective blanket exists; the converse is true at 1600°C.

An apparent activation energy for a temperature-controlled rate process can be determined by plotting the log of the rate vs the reciprocal of the absolute temperature. Figure 12 shows this relationship for 11.7 w/o C ZrC, from which the activation energy is determined to be 16.3 kcal/mole. The activation energy for oxidation of ZrC has received limited attention. Margrave and Kuriakose (Ref. 1) have reported a value of 16.7 kcal/mole, and Bartlett (Ref. 2) has reported a value of 45.7 kcal/mole. The activation energy in this study comes surprisingly close to that of Margrave and Kuriakose, considering the differences in experimental procedure.

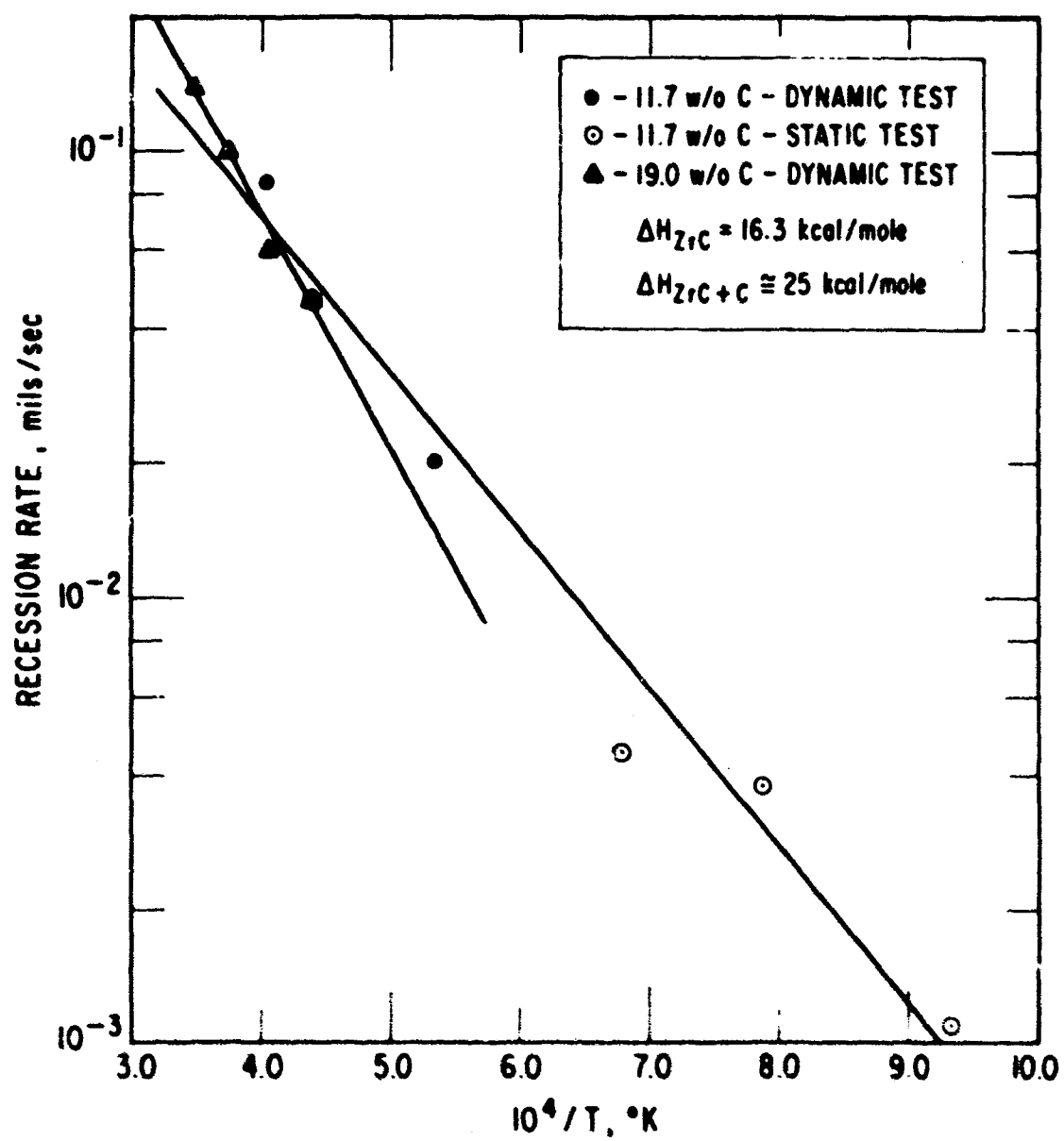


Fig. 12. Recession Rate vs  $1/T$  for  $ZrC$  and  $ZrC + C$



The data for 19.0 w/o C are also plotted in Fig. 12. The activation energy for the higher C percentage is calculated to be 24.2 kcal/mole. Thus, as the C content is increased, resulting in free graphite in the microstructure, the apparent activation energy increases above the single-phased carbide, approaching that of graphite (~ 40 kcal/mole).

#### B. EFFECT OF ALLOYING ADDITIONS

The addition of alloying elements to ZrC had little effect, either on the static or on the dynamic oxidation behavior compared with the effect of carbon. In most cases, it was not possible to determine whether the change in oxidation behavior was due to the effect of the alloying addition or to the uncertainty in the carbon concentration. In the static tests, no alloying addition showed superior oxidation resistance throughout the temperature range studied. At 800 and 1000°C, Ta and B appeared to look good, but at 1200°C the base carbide had a lower recession rate than any of the alloyed carbides.

In the dynamic tests, the alloyed carbides had approximately the same recession rates as the unalloyed carbides of the same carbon composition. Again, no alloying addition showed superior oxidation behavior.

#### C. EFFECT OF IRON

A comparison of the static oxidation of hot-pressed ZrC of eutectic composition both with and without Fe showed that there was little difference in the oxidation characteristics of the samples. The Fe was found in the microstructure as  $\text{Fe}_3\text{C}$ . Since the hot-pressing was carried out at a temperature well above the melting point of  $\text{Fe}_3\text{C}$ , the phase was liquid during pressing and solidified in the ZrC grain boundaries. The oxidation of the  $\text{Fe}_3\text{C}$  was somewhat more rapid than the ZrC, as can be seen in Fig. 13 where the intergranular  $\text{Fe}_3\text{C}$  has been attacked well into the ZrC matrix.

Attempts to determine the dynamic oxidation characteristics of Fe-free, hot-pressed, eutectic ZrC failed, but they pointed out that the presence of  $\text{Fe}_3\text{C}$  in the microstructure could be useful. Attempts to heat



Fig. 13. Oxidation of Intergranular  $\text{Fe}_3\text{C}$  in  $\text{ZrC}$  Matrix

these specimens to even the lowest oxidation test temperature failed, as the samples cracked during heating due to thermal shock. Apparently, the  $\text{Fe}_3\text{C}$  in the grain boundaries allowed some relief of stress resulting from thermal expansion so that the Fe-contaminated material was not susceptible to thermal shock, even as the monocarbide. It appears that the only effect of the Fe on the oxidation resistance is to decrease the resistance slightly.

#### D. COMPARISON OF ZrC AND W

One of the principal difficulties of dynamic oxidation testing is the problem of comparison of materials. There is a large number of variables in oxidation testing. Unless the variables can be specified, no comparison between materials can be made unless an identical test procedure is followed.

In this program, the dynamic test apparatus was the same as that used in a developmental program to improve the oxidation resistance of W alloys (Ref. 3).

The alloy which showed the greatest improvement over unalloyed W was an alloy of W + 10 v/o  $\text{Al}_2\text{O}_3$ . The data from Ref. 3 for pure W and W + 10 v/o  $\text{Al}_2\text{O}_3$  are plotted in Fig. 14 along with the data for ZrC with 19.0 w/o C. It can be seen that the recession rate of the ZrC is considerably lower throughout the entire temperature range, approaching an order of magnitude at  $2800^\circ\text{C}$ . The reason that the carbide curve does not increase as rapidly at the higher temperatures as does the W curve is that the oxide is retained in the case of the carbide, but is volatile in the case of W. This continually exposes W to the oxidizing environment, while the carbide can form a protective coating of oxide and the trapped CO must diffuse through the pores of the oxide to allow oxidation to continue.

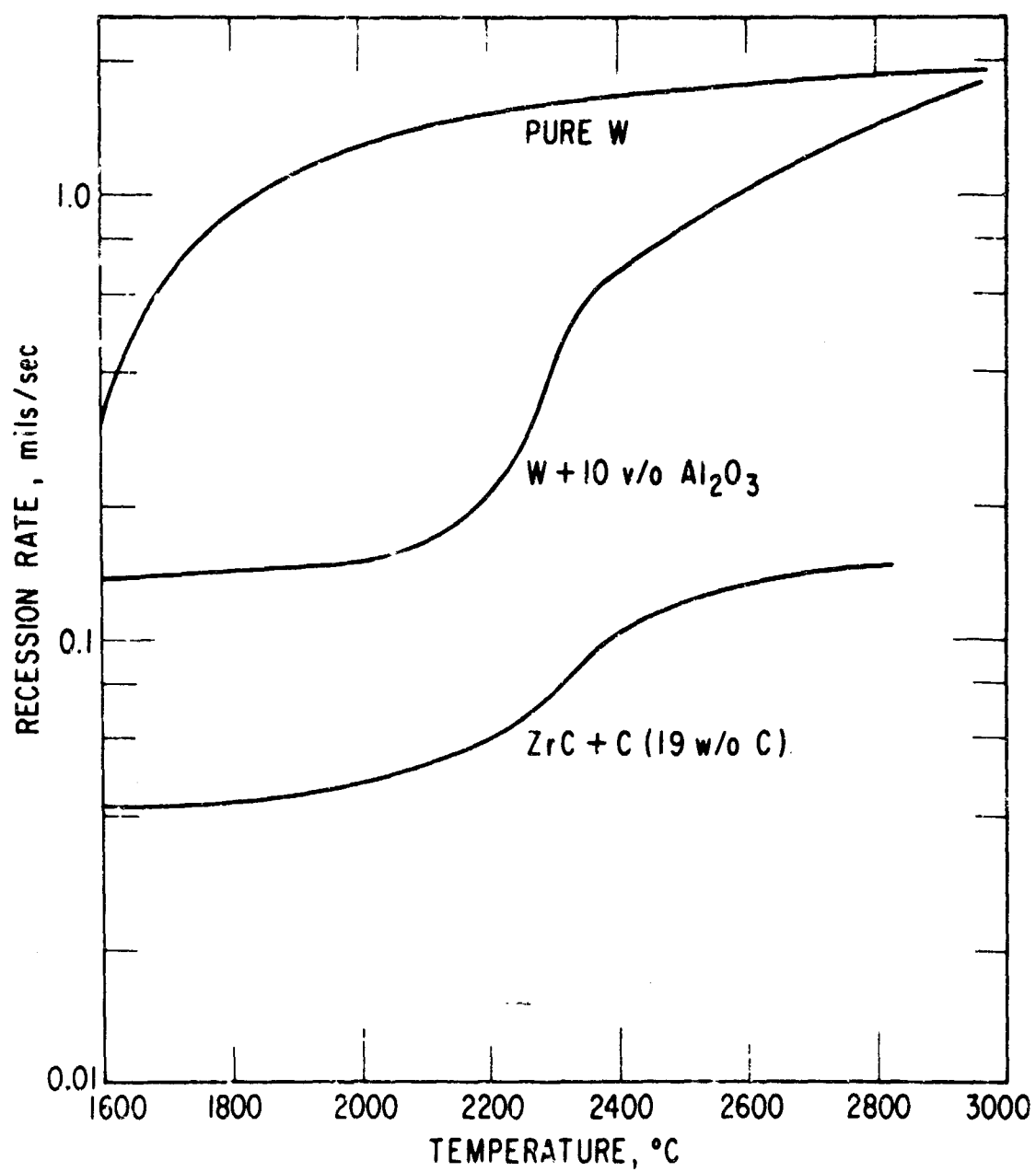


Fig. 14. Comparison of Recession Rates of 19 w/o C ZrC With Pure W and W + 10 v/o Al<sub>2</sub>O<sub>3</sub>

## V. CONCLUSIONS

The oxidation behavior of single-phased ZrC and ZrC + C is strongly dependent upon the C concentration. At lower temperatures increasing the carbon content decreases the resistance to oxidation. At higher temperatures, effusion through the oxide layer is the rate-controlling factor and the presence of free graphite forms CO which must diffuse outward, decreasing the amount of oxygen reaching the surface and lowering the oxidation rate. An apparent activation energy of oxidation of ZrC of 11.7 w/o C was found to be 16.3 kcal/mole in the temperature range of 800-2200°C. Increasing the C content to give free graphite also increased the activation energy of oxidation.

Alloying additions, including B, Cr, Ta, and ThO<sub>2</sub>, had little effect on either the static or the dynamic oxidation behaviors.

The oxidation behavior of unalloyed ZrC, when compared with pure W and a W alloy developed for good oxidation resistance, showed that the ZrC had recession rates approaching an order of magnitude lower than the W alloy, both materials being tested under identical conditions.

#### REFERENCES

1. A. K. Kuriakose and J. L. Margrave, Thermodynamic and Kinetic Studies for a Refractory Materials Program, ASD-TDR-62-204, Part II, Aeronautical Systems Division, Wright-Patterson Air Force Base, Ohio, (May 1963), p. 98.
2. R. W. Bartlett, Dissertation Abstr. 22, (11), 3973 (1961-62).
3. J. E. White, Development of Oxidation Resistant Tungsten-Base Alloys, TDR-469 (5250-10)-9, Aerospace Corporation, El Segundo, California, (April 1965).